Title

Spark Plasma Sintering Apparatus Used for the Formation of Strontium Titanate Bicrystals.

Journal

Journal of Visualized Experiments, 2017(120)

ISSN

1940-087X

Authors

Hughes, Lauren A
van Benthem, Klaus

Publication Date

2017

DOI

10.3791/55223

Peer reviewed

Video Article

Spark Plasma Sintering Apparatus Used for the Formation of Strontium Titanate Bicrystals

Lauren A. Hughes[1], Klaus van Benthem[1]

[1]Department of Materials Science and Engineering, University of California, Davis

Correspondence to: Klaus van Benthem at benthem@ucdavis.edu

URL: https://www.jove.com/video/55223
DOI: doi:10.3791/55223

Keywords: Engineering, Issue 120, grain boundary, bicrystal, electric field, spark plasma sintering, strontium titanate, scanning transmission electron microscopy

Date Published: 2/9/2017

Citation: Hughes, L.A., van Benthem, K. Spark Plasma Sintering Apparatus Used for the Formation of Strontium Titanate Bicrystals. *J. Vis. Exp.* (120), e55223, doi:10.3791/55223 (2017).

Abstract

A spark plasma sintering apparatus was used as a novel method for diffusion bonding of two single crystals of strontium titanate to form bicrystals with one twist grain boundary. This apparatus utilizes high uniaxial pressure and a pulsed direct current for rapid consolidation of material. Diffusion bonding of strontium titanate bicrystals without fracture, in a spark plasma sintering apparatus, is possible at high pressures due to the unusual temperature dependent plasticity behavior of strontium titanate. We demonstrate a method for the successful formation of bicrystals at accelerated time scales and lower temperatures in a spark plasma sintering apparatus compared to bicrystals formed by conventional diffusion bonding parameters. Bond quality was verified by scanning electron microscopy. A clean and atomically abrupt interface containing no secondary phases was observed using transmission electron microscopy techniques. Local changes in bonding across the boundary was characterized by simultaneous scanning transmission electron microscopy and spatially resolved electron energy-loss spectroscopy.

Video Link

The video component of this article can be found at https://www.jove.com/video/55223/

Introduction

Spark plasma sintering (SPS) is a technique in which application of high uniaxial pressure and pulsed direct current leads to the rapid densification of powder compacts[1]. This technique also leads to the successful formation of composite structures from various materials, including silicon nitride/silicon carbide, zirconium boride/silicon carbide, or silicon carbide, with no additional sintering aids required[2,3,4,5]. The synthesis of these composite structures by conventional hot-pressing had been challenging in the past. While application of a high uniaxial pressure and fast heating rate via the SPS technique enhances consolidation of powders and composites, the phenomenon causing this enhanced densification debated in the literature[2,3,6,7]. There also exists only limited information regarding the influence of electric fields on grain boundary formation and the resulting atomic structures of grain boundary cores[8,9]. These core structures determine the functional properties of SPS sintered materials, including electric breakdown of high voltage capacitors and the mechanical strength and toughness of ceramic oxides[10]. Therefore, understanding the fundamental grain boundary structure as a function of SPS processing parameters, such as applied current, is necessary for the manipulation of a material's overall physical properties. One method to systematically elucidate the fundamental physical mechanisms underpinning SPS is the formation of specific grain boundary structures, *i.e.*, bicrystals. A bicrystal is created by manipulation of two single crystals, which are then diffusion bonded with specific misorientation angles[11]. This method provides a controlled way to investigate the fundamental grain boundary core structures as a function of processing parameters, dopant concentration, and impurity segregation[12,13,14].

Diffusion bonding is dependent on four parameters: temperature, time, pressure, and bonding atmosphere[15]. Conventional diffusion bonding of strontium titanate ($SrTiO_3$, STO) bicrystals typically occurs at a pressure below 1 MPa, within a temperature range of 1,400-1,500 °C, and time scales ranging from 3 to 20 hours[13,14,16,17]. In this study, bonding in a SPS apparatus is achieved at significantly lower temperature and time scales in comparison to conventional methods. For polycrystalline materials, reduced temperature and time scales via SPS significantly limits grain growth, thereby providing advantageous control of a material's properties through manipulation of its microstructure.

The SPS apparatus, for a 5×5 mm^2 sample, exerts a minimum pressure of 140 MPa. Within the conventional diffusion bonding temperature range, Hutt *et al.* report instantaneous fracture of STO when the bonding pressure exceeds 10 MPa[18]. However, STO exhibits temperature dependent plasticity behavior, indicating bonding pressure can exceed 10 MPa at specific temperatures. Above 1,200 °C and below 700 °C, STO exhibits some ductility, at which stresses greater than 120 MPa can be applied without instantaneous fracture of the sample. Within the intermediate temperature range of 700-1,200 °C, STO is brittle and experiences instantaneous fracture at stresses greater than 10 MPa. At 800 °C, STO has minor deformability prior to fracture at stresses less than 200 MPa[19,20,21]. Hence, bonding temperatures for STO bicrystal formation via SPS apparatus must be selected according to the plasticity behavior of the material.

Protocol

1. Sample Preparation of Single Crystal Strontium Titanate

NOTE: Single crystal STO is supplied with a (100) surface polished to a mirror finish.

1. Section STO into 5x5 mm^2 pieces using diamond wire saw.
2. Ultrasonically clean samples at 50-60 Hz consecutively in baths of acetone, isopropanol, and methanol for fifteen minutes each.
3. Remove STO from methanol bath to immediately place on hot plate held at a temperature of 200 °C. Heating the sample after cleaning prevents formation of evaporation spotting from the alcohol.
4. Place samples for ten minutes in buffered hydrofluoric acid (pH=4), a 6:1 solution of ammonium fluoride and 49% hydrofluoric acid.[22] This solution etches the STO, forming a predominantly (100) TiO_2 terminated surface. If the optically flat side of the single crystal has a rainbow patina, the sample has been over-etched and should not be used.
5. After ten minutes in the etchant solution, rinse samples in deionized (DI) water and then in isopropanol. Dry using clean house air.

2. Bicrystal Formation via Spark Plasma Sintering Apparatus

NOTE: For 5x5 mm^2 crystal use a 30 mm diameter graphite die. If a die with a diameter smaller than 30 mm is used, the bicrystal catastrophically fractures during bonding. Optimal die size as well as pressure exerted by the SPS apparatus is highly dependent on the size of the crystals.

1. Place a 30 mm circle of graphite paper on a graphite plunger with a 30 mm diameter. Graphite paper prevents STO from bonding to the graphite plunger during the experiment.
2. Stack two 5x5 mm^2 STO single crystals with their optically flat surfaces placed facing inward to form the bicrystal boundary. Center the stack on top of the graphite paper and plunger.
3. Rotate the top single crystal around the <100> axis to a chosen misorientation angle. The <100> axis is perpendicular to the optically flat surface of crystal.
4. Slide the graphite die over the plunger and crystals. Place a second 30 mm diameter circle of graphite paper and then 30 mm diameter plunger over the stacked STO crystals.
5. Stack the combined plungers and die onto the graphite spacers in SPS apparatus (**Figure 1**).
6. Apply a uniaxial force of 3 kN to minimize contact resistance using the z-axis control buttons. Throughout the experiment, the user must keep the force at 3 kN via the z-axis control buttons.
7. Insert k-type thermocouple into graphite die at the small hole, shown in **Figure 1**. The thermocouple extends through the die to the sample.
8. Set the chamber pressure of the SPS apparatus to ~10 Pa using the vacuum push buttons.
9. Select bond temperature, time, and heating rates via program instrument control software (**Table 1**). For the bonding temperature and time, use a heating rate of 70-80 °C/min and a cooling rate of 50 °C/min.
10. Set 12 s on, 2 s off DC pulse using the instrument sintering button. A pulsed bias of ~ 4 V and direct current of ~550 A are applied incrementally to the sample once the program is set to run.
11. Press the start button on the machine.
12. Remove the sample when the program ends. After bicrystal formation, the sample will appear grey-black due to the reducing environment of the SPS apparatus.
13. Use a high temperature furnace at a temperature of 1,200 °C for 140 h, apply no pressure during this procedure, to anneal and re-oxidize the sample in air. Annealing parameters were selected according to previous work done by Hutt *et al*. in which bicrystals formed in high vacuum[13]. After annealing, the sample reveals an off-white color and is oxidized.

3. Sample Preparation of Bicrystal for Electron Beam Imaging

1. Cross-section bicrystal with diamond wire saw into 5x1 mm^2 sections.
2. Polish cross-section samples with diamond lapping film. The grit size on the diamond lapping film is gradually decreased from 9 µm to 0.1 µm. Change to smaller grit size once scratches are uniform across the surface. Use a counter clockwise platen motion for 9 µm to 6 µm lapping film. Use a counter clockwise platen motion with an oscillating sample head for 6 µm to 0.1 µm lapping film.
3. Polish cross-section samples with colloidal silica for two minutes using a mat cloth. Continuously pour colloidal silica onto the mat with counter clockwise platen motion and oscillating sample head.
4. Fifteen seconds before removing the sample, stop pouring colloidal silica and pour DI water onto platen. Pour DI water for fifteen seconds, remove sample, and immediately rinse sample in DI water for 1 min. If this procedure is not followed, the colloidal silica will bond the sample's surface and obscure the grain boundary during scanning electron microscopy (SEM).
5. Once the sample is polished to an optically smooth surface, ultrasonically clean samples consecutively in baths of acetone, isopropanol, and methanol for fifteen minutes each.
6. Remove STO from methanol bath to immediately place on hot plate held at a temperature of 200 °C. Heating the sample after cleaning prevents formation of evaporation spotting from the alcohol.
7. Mount sample polished surface up onto a sample stub using colloidal graphite.
8. Sputter coat sample surface with 2-3 nm of carbon. Use the following parameters for the carbon coater: a pulse resolution of 0.2 nm/pulse, current step rate of 0.2 A/pulse, pulse current of 40 A, pulse length of 2 s, and maximum pulses of 50.

4. Cleaning the FIB Copper Grid

NOTE: Improper cleaning of the FIB grid can lead to carbon contamination of the lamella in the TEM.

1. Place copper FIB grid in an acetone and then isopropanol bath for 1 h each.
2. Plasma clean copper FIB grid for 10 min.

5. Preparation of Transmission Electron Microscopy (TEM) Lamella via Focused Ion Beam (FIB) Apparatus

NOTE: All parameters used in FIB preparation are typed or selected from a drop down menu in the FIB apparatus software.

1. Place STO sample and copper FIB grid in FIB apparatus. The stage is at 7 mm.
2. Find a region of interest along the interface between the two single crystals, *i.e.*, the grain boundary.
3. Select Patterning dialogue box. In Patterning Control, select the Rectangle Patterning Tool with application property C-e-dep surface. Insert C-dep for gas injection. Deposit a 15×2×2 μm^3 protective layer of carbon using the electron beam at a voltage of 5.0 kV, a current of 13.0 nA, and a tilt angle of 0°. Retract C-dep.
4. Select Patterning dialogue box. In Patterning Control, select the Rectangle Patterning Tool with application property W-dep. Insert W-dep for gas injection. Deposit 15×2×2 μm^3 protective layer of tungsten using the ion beam at a voltage of 30.0 kV, a current of 0.3 nA, and a tilt angle of 52°. Retract W-dep.
5. Select Patterning dialogue box. In Patterning Control, select the Regular Cross Section Patterning Tool with application property Si. Use 22×25×15 μm^3 for the bottom pattern and of 22×27×15 μm^3 for the top pattern at a voltage of 30.0 kV, a current of 30.0 nA, and a tilt angle of 52° via the ion beam. The pattern will create a trench mill on both sides of the protective layer.
6. Select Patterning dialogue box. In Patterning Control, select the Clean Cross Section Patterning Tool with application property Si. Use 22×3×60 μm^3 for the top and bottom pattern at a voltage of 30.0 kV and a current of 1.0 nA via the ion beam. The tilt angle is 53.5° for the bottom pattern and 50.5° for the top pattern. The pattern cleans the surface of the trenched lamella from the curtaining pattern that results from the regular cross section patterning.
7. Cut a J-pattern into the sample using the Rectangle Patterning tool with application property Si. Use 2 µm for the width at a voltage of 30.0 kV and a current of 1.0 nA via the ion beam.
8. Select Easy Lift dialogue box. Insert the micromanipulator to the park position. Lower the micromanipulator and attach the sample to the copper FIB grid via a tungsten weld using the process detailed in 5.4.
9. Using the steps detailed in 5.7, µcut a U-pattern, continuing from the original J-pattern, in the sample using the ion beam at a voltage of 30.0 kV and a current of 1.0 nA.
10. Lift the lamella via the micromanipulator above the bulk sample.
11. Rotate the micromanipulator 180°, so the grain boundary is no longer parallel to ion beam, but perpendicular to the ion beam.
12. Tungsten weld the lamella to a copper FIB grid using the steps detailed in 5.4 with the ion beam at a voltage of 30.0 kV and a current of 0.3 nA.
13. Cut the micromanipulator from the lamella using the steps detailed in 5.7 with the ion beam at a voltage of 30.0 kV and a current of 1.0 nA.
14. Repeat the steps detailed in 5.3. Deposit a 15×2×4 μm^3 protective layer of carbon using an electron beam at a voltage of 5.0 kV, a current of 13.0 nA, and a tilt angle of 0°.
15. Repeat the steps detailed in 5.4. Deposit 15×2×8 μm^3 protective layer of tungsten using an ion beam at a voltage of 30.0 kV, a current of 0.3 nA, and a tilt angle of 52°.
16. With the ion beam, thin the sample to approximately 200 nm using a voltage of 30.0 kV and a systematically decreasing current of 0.5 nA, 0.3 nA, and 0.1 nA. At this stage, a cleaning cross section pattern is used and the sample is tilted to an angle of 52 ±± 1.5°.
17. With the ion beam, thin the sample to electron transparency using a voltage of 5.0 kV and a current of 77.0 pA. At this stage, a rectangle pattern is used with a tilt angle of 52 ± 3°.
18. Remove amorphous damage incurred from the FIB by cleaning the sample at a voltage of 500 eV and a current of 150 µA.
19. Place TEM sample in TEM holder and insert holder in scanning transmission electron microscope (STEM). Select 'Capture', image sample grain boundary.

Representative Results

Bonding temperature, time, and misorientation angle were all altered to determine optimum parameters needed for the maximum possible bonded interface fraction of the STO bicrystal (**Table 1**). The interface was considered 'bonded' when the grain boundary was not visible during SEM imaging (**Figure 2a**). A 'non-bonded' interface was exhibited when a dark image contrast or voids were present at the boundary location (**Figure 2b**). Dark image contrast signified colloidal graphite from the FIB mounting procedure had diffused between the two STO crystals due to capillary effects. This non-bonded interface is observed at the edges of the bicrystal, while the bonded interface is observed at the center of the bicrystal. The change in bonding behavior from the edge to the center of the bicrystals formed by SPS apparatus is also seen in bicrystals formed via hot pressing techniques[6].

Micro-crack formation in the bulk of the bicrystal is observed in all samples. For successfully bonded bicrystals, micro-crack formation does not interfere with the bonded interface. At a bonding temperature of 1,200 °C, extensive micro-cracking occurs, leading to brittle failure of the bicrystal during annealing. Therefore, bonding temperature in the SPS apparatus was kept below 800 °C to prevent catastrophic fracture.

For bicrystals with 0° misorientation angle at bonding temperatures of 600 °C and 700 °C, a 95% successfully bonded interface was obtained. An increase in the misorientation angle of the bicrystal to 44.4° requires a bonding temperature of 800 °C and bonding time of 90 minutes to achieve a 45.8% successfully bonded interface. High resolution TEM (HRTEM) and high angle annular dark field scanning transmission electron microscopy (HAADF-STEM) micrographs of this sample reveal an atomically abrupt grain boundary structure with no intergranular film or secondary phases present (**Figure 3**). Spatially resolved electron energy loss spectroscopy (EELS) recorded directly from the interface shows a reduction in the crystal field splitting of the Ti L_3 and L_2 edges as well as a reduction in the O K edge intensity when compared to the bulk (**Figure 4**).

Bicrystal	Twist Orientation (°)	Bond Temperature (°C)	Bond Time (min)	Anneal Temperature (°C)	Anneal Time (h)	Bonded Interface ± 0.3 (%)
A	0*	1200	15	1,200	16	--
B	0	600	90	1,200	100	92.3
C	0	700	90	1,200	100	99.7
D	4.3 ± 0.3	800	20	1,200	50	79.2
E	45*	700	60	1,200	140	1.3
F	46.1 ± 0.5	800	20	1,200	140	35.4
G	44.4 ± 0.1	800	90	1,200	140	45.8

Table 1. Bonding Parameters and Subsequent Interface Fraction of Bicrystals. SPS apparatus diffusion bonding parameters and subsequent bonded interface fractions of STO bicrystals. A pulsed bias voltage of ~4 V and direct current of ~550 A is applied for all experiments. Bonded interface fractions were calculated from an average grain boundary length of (1.5 ± 0.4) mm. These regions were taken from varying areas within the bicrystal.

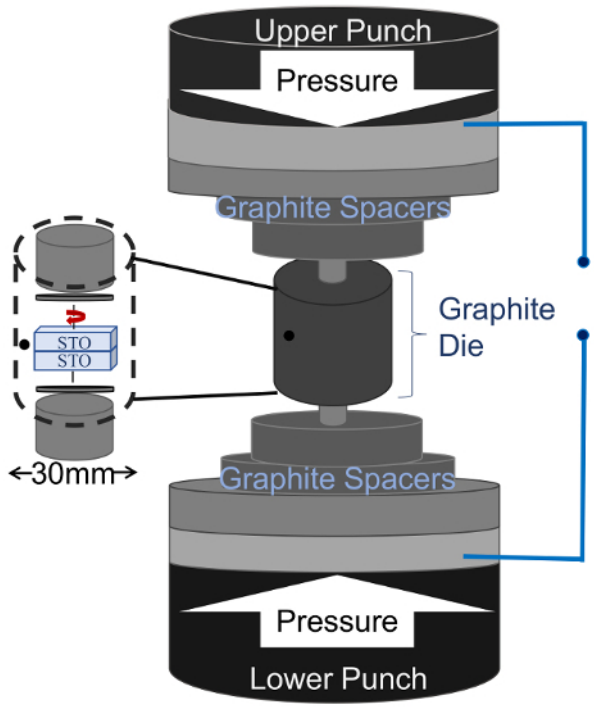

Figure 1. Spark Plasma Sintering Apparatus. Set up for the spark plasma sintering apparatus. Pressure is applied perpendicular to the bicrystal interface. Please click here to view a larger version of this figure.

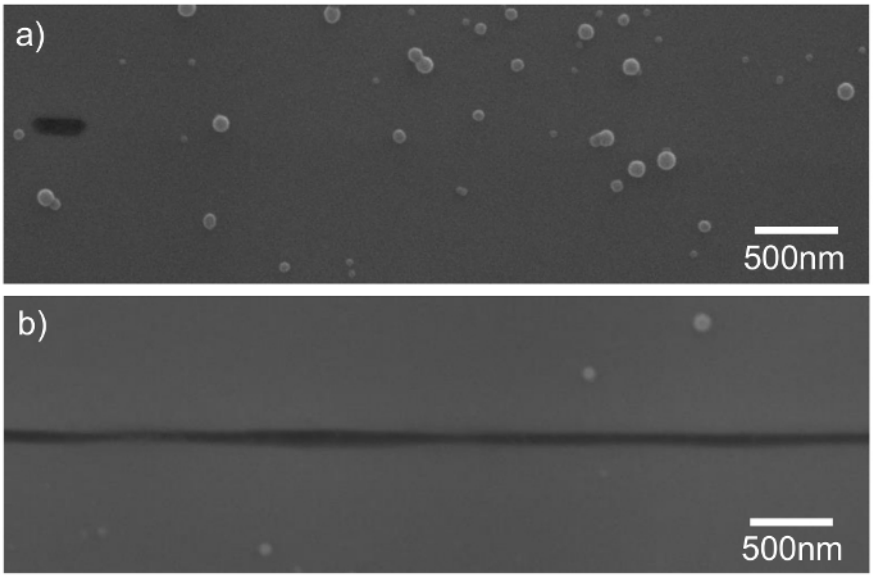

Figure 2. Typical Interfaces Found in SPS Apparatus Formed Bicrystals. Nominal 45° twist bicrystal formed at a temperature of 800 °C for 90 minutes. (**a**) SEM image of defined 'bonded' interface, the grain boundary location is inferred by the presence of a faceted void, and (**b**) SEM image of the defined 'non-bonded' interface. Spherical beads observed in images are residual silica from polishing. Please click here to view a larger version of this figure.

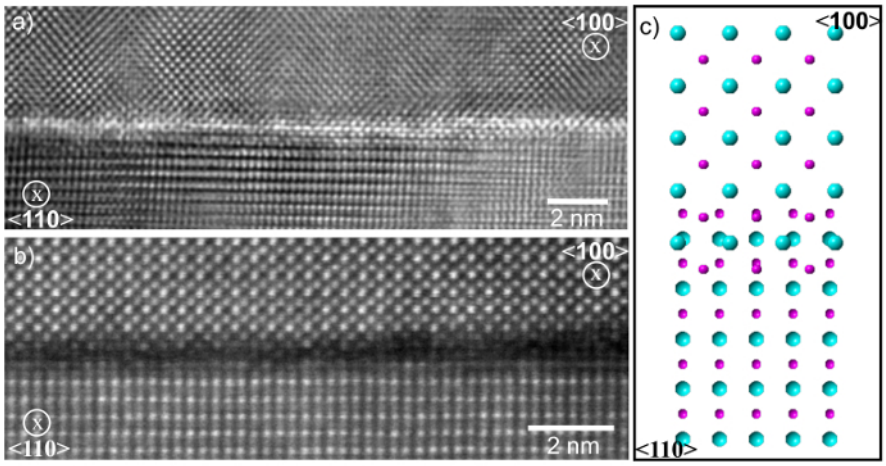

Figure 3. High Resolution Imaging of Bicrystal Grain Boundary. Boundary of nominal 45° twist bicrystal formed at a temperature of 800 °C for 90 minutes recorded in <100> zone axis with an edge-on orientation for the interface plane. (**a**) HRTEM image, (**b**) HRSTEM DF image, and (**c**) structure model composed of two single crystals, one in <100> and one in <110> zone axis orientation with a {001} interface plane. Deviations of the experimental imaging data from the projected structure model represent changes of the interface configuration compared to the ideal single-crystal atom positions. Please click here to view a larger version of this figure.

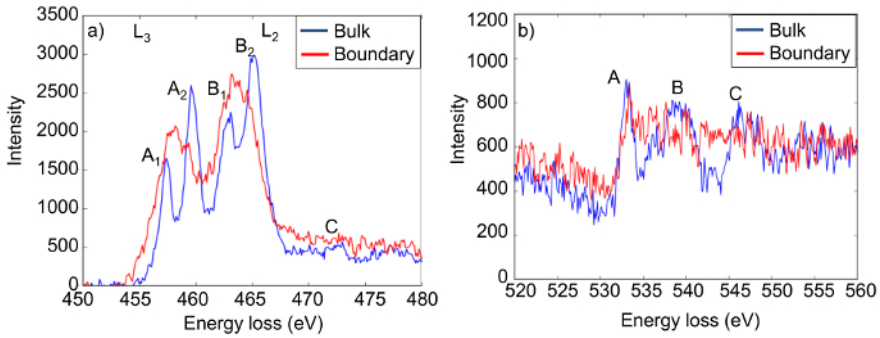

Figure 4. Structure and Chemistry of Bicrystal Grain Boundary. Near edge fine structure of (**a**) the Ti $L_{2,3}$ edge and (**b**) the O K edge taken at the boundary and the bulk of 45° twist bicrystal formed at a temperature of 800 °C for 90 minutes. Please click here to view a larger version of this figure.

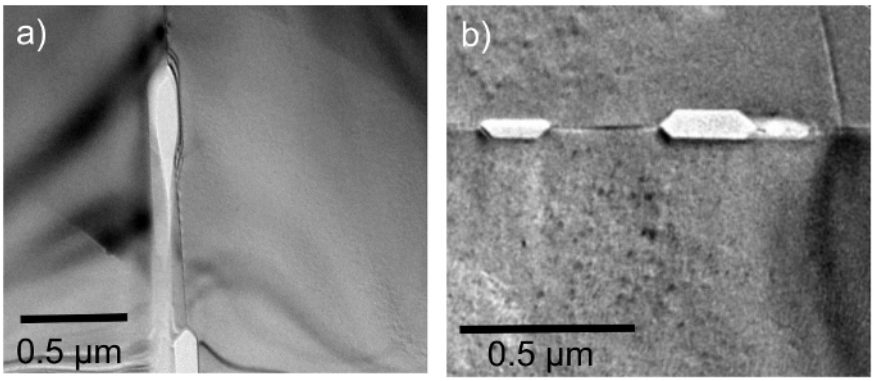

Figure 5. FIB Milling at Bicrystal Grain Boundary. HRTEM images of FIB TEM lamella of (**a**) sample with grain boundary parallel to the ion beam and (**b**) sample with grain boundary perpendicular to the ion beam. Please click here to view a larger version of this figure.

Discussion

The bonding temperature of 1,200 °C was chosen to maximize diffusion as small changes in temperature can greatly impact the kinetics of all diffusion bonding mechanisms. A temperature of 1,200 °C is outside the brittle-ductile transition temperature range of STO. However, the sample underwent brittle fracture at this temperature. The catastrophic failure of the STO bicrystal was not unexpected as STO has ~ 0.5% ductility at 1,200 °C. Also, the sample was held at a pressure of 140 MPa throughout the heating process and STO transitions through its brittle stage during this heating process where it has 0% ductility[21]. Thus successful diffusion bonding of single crystals via the SPS apparatus necessitates an in-depth understanding of the temperature dependent plasticity behavior of a material.

Two bicrystals were formed using a bonding temperature of 800 °C and a bonding time of 20 minutes. The bicrystal with a nominal misorientation of 4˚ was annealed for 50 hours and exhibited a bonded interface fraction 2.2x greater than the bicrystal with nominal misorientation of 45°, annealed for 140 hours. Annealing times longer than 50 hours did not reveal any significant improvement of the diffusion bonding quality. Annealing temperature and time were selected according to previous work in which the bicrystals were formed in a high vacuum furnace, similar to the SPS apparatus[11]. To ascertain if there was an impact of the annealing process on the diffusion bonding of these bicrystals, diffusion bond lengths were calculated and found to be 0.27 nm at a temperature of 1,200 °C for 140 hours[23]. The selected annealing parameters, therefore, only had limited impact on the diffusion bonding of the bicrystal. This analysis was further supported when the diffusion bonding of a bicrystal with a 45° twist misorientation was not successful for the same parameters utilized during annealing.

While the selected annealing parameters did not significantly impact the diffusion bonding, the misorientation angle does have a pronounced effect. High-angle misorientation angles create a greater structural mismatch between the two half-crystals, which hinders cross diffusion and decreases interface bonding. For high misorientation angles, bonding temperature and time must be increased in order to have a larger successfully bonded interface fraction.

Bicrystal formation via SPS processing techniques occurs at significantly accelerated times scales and moderate temperature ranges compared to the conventional hot press methods. This difference in processing parameters between conventional diffusion bonding and the SPS method is also seen in the formation of powder compacts and composites. As mentioned above, bicrystals formed via conventional diffusion bonding methods are formed at temperatures greater than 1,400 °C with times scales ranging from 3 to 20 hours[11,24]. Using a SPS instrument, diffusion bonding occurs at a temperature of 800 °C with times scales ranging from 20 to 90 minutes. The SPS technique is then useful for the rapid diffusion bonding of bicrystals compared to conventional methods. Bicrystal formation by the SPS instrument also allows for experimental observation of the mass transfer mechanisms at a grain boundary with a selected misorientation. This experimental observation will provide more insight into the mechanisms underpinning the SPS technique.

Micro-cracks in the bulk STO bicrystal prevented conventional mechanical TEM lamella preparation. The mechanical thinning process led to fracture of the TEM lamella due to micro-cracks spreading throughout the bulk. Therefore, FIB preparation of the TEM lamella was used. Conventional FIB lift-out of the lamella, in which the grain boundary is parallel to the ion beam, led to preferential milling along the interface plane (**Figure 5a**). The FIB preparation technique was subsequently modified. First, the thickness of the initial protective layer of carbon and tungsten was selected so, at the end of the lift-out step, the protective layer was milled away. If the protective layer was too thick and remained throughout the thinning process, re-deposition of tungsten occurred and obscured TEM analysis. Secondly, after the TEM lamella was attached to the tip of the micromanipulator, the micromanipulator was rotated by 180°. This rotation caused the grain boundary to become perpendicular to the ion beam, hence preventing preferential thinning (**Figure 5b**). Lastly, after the lift-out process, protective layers of carbon and tungsten were deposited onto the surface of the newly oriented TEM lamella. These modifications to the conventional FIB preparation technique led to a clean TEM lamella enabling atomically resolution imaging by HAADF-STEM.

HRTEM and HAADF-STEM micrographs for the bicrystal bonded at 800 °C for 90 minutes with a nominal 45° twist grain boundary show an atomically resolved grain boundary structure with no secondary phases. Spatially resolved EELS reveal changes in the Ti coordination within the grain boundary cores, indicating an increase in the oxygen vacancy concentration compared to the bulk. These results are consistent with reports in the literature for low-angle twist grain boundaries[25]. Further analysis of these experiments is described elsewhere[26].

In this study, STO bicrystals were successfully synthesized for the first time using a SPS apparatus. Bicrystals with twist orientations of 0°, 4°, and 45° were formed at high pressure with moderate bonding temperatures and time scales compared to those parameters found in conventional bonding. Formation of bicrystals via the SPS apparatus provides an opportunity to quantitatively determine the impact of electric field as well as heating rate on selected grain boundary core structures.

Disclosures

We have nothing to disclose.

Acknowledgements

LH gratefully acknowledges financial support by an US National Science Foundation Graduate Research Fellowship under Grant No. 1148897. Electron microscopy characterization and SPS processing at UC Davis was financially supported by a University of California Laboratory Fee award (#12-LR-238313). *Work at the Molecular Foundry was supported by the Office of Science, Office of Basic Energy Sciences, of the U.S. Department of Energy under Contract No. DE-AC02-05CH11231.*

References

1. Munir, Z. A., Anselmi-Tamburini, U., & Ohyanagi, M. The effect of electric field and pressure on the synthesis and consolidation of materials: A review of the spark plasma sintering method. *J. Mater. Sci.* **41** (3), 763-777 (2006).
2. Chen, W., Anselmi-Tamburini, U., Garay, J. E., Groza, J. R., & Munir, Z. A. Fundamental investigations on the spark plasma sintering/synthesis process: I. Effect of dc pulsing on reactivity. *Mater. Sci. Eng. A.* **394** (1-2), 132-138 (2005).
3. Holland, T. B., Anselmi-Tamburini, U., & Mukherjee, A. K. Electric fields and the future of scalability in spark plasma sintering. *Scr. Mater.* **69** (2), 117-121 (2013).
4. Wan, J., Duan, R., & Mukherjee, A. Spark plasma sintering of silicon nitride/silicon carbide nanocomposites with reduced additive amounts. *Scr. Mater.* **53** (6), 663-667 (2005).
5. Carney, C. M., Mogilvesky, P., & Parthasarathy, T. A. Oxidation Behavior of Zirconium Diboride Silicon Carbide Produced by the Spark Plasma Sintering Method. *J. Amer. Ceram. Soc.* **92** (9), 2046-2052 (2009).
6. Dupeux, M. Production of Oriented Two-Phase Bicrystals by Diffusion Bonding Technique. *J. Cryst. Growth.* **66** 169-178 (1984).
7. Castro, R., & van Benthem, K. *Sintering: mechanisms of convention nanodensification and field assisted processes.* **35** Springer Science & Business Media (2012).
8. Byeon, S. C., & Hong, K. S. Electric field assisted bonding of ceramics. *Mater. Sci. Eng. A.* **287** (2), 159-170 (2000).
9. Wang, J., & Conrad, H. Contribution of the space charge to the grain boundary energy in yttria-stabilized zirconia. *J. Mater. Sci.* **49** (17), 6074-6080 (2014).
10. Fujimoto, M., & Kingery, W. D. Microstructures of SrTiO3 Internal Boundry Layer Capacitors During and After Processing and Resultant Electrical Properties. *J. Amer. Ceram. Soc.* **68** (4), 169-173 (1985).
11. Mitsuma, T. *et al.* Structures of a Σ = 9, [110]/{221} symmetrical tilt grain boundary in SrTiO3. *Journal of Materials Science.* **46** (12), 4162-4168 (2011).
12. Ikuhara, Y. Grain Boundary and Interface Structures in Ceramics. *J. Ceram. Soc. Jpn.* **109** (7), S110-S120 (2001).
13. Hutt, S., Kienzle, O., Ernst, F., & Ruhle, M. Processing and Structure of Grain boundaries in Strontium Titanate. *Z. Metallkd.* **92** (2), 105-109 (2001).
14. Takahisa, Y., Ikuhara, Y., & Sakuma, T. Current-voltage characteristics across 45◦ symmetric tilt boundary in highly donor-doped SrTiO3 bicrystal. *J. Mater. Sci. Lett.* **20** 1827-1829 (2001).
15. Hill, A., & Wallach, E. R. Modelling Solid State Diffusion Bonding. *Acta Metall.* **37** (9), 2425-2437 (1989).
16. Sato, Y. *et al.* Non-linear current-voltage characteristics related to native defects in SrTiO3 and ZnO bicrystals. *Sci. Technol. Adv. Mater.* **4** (6), 605-611 (2003).
17. Hirose, S., Nishimura, H., & Niimi, H. Resistance switching effect in Nb-doped SrTiO[sub 3] (100) bicrystal with (100) #45° twist boundary. *J. App. Phys.* **106** (4), 043714-043711-043716 (2009).
18. Hutt, S. Doctoral Thesis. *University of Stuttgart.* (2002).
19. Brunner, D., Taeri-Baghbadrani, S., Sigle, W., & Ruhle, M. Suprising Results of a Studay on the Plasticity in Strontium Titanate. *J. Amer. Ceram. Soc.* **84** (5), 1161-1163 (2001).

20. Gumbsch, P., Taeri-Baghbadrani, S., Brunner, D., Sigle, W., & Ruhle, M. Plasticity and an inverse brittle-to-ductile transition in strontium titanate. *Phys. Rev. Lett.* **87** (8), 085505-085501-085504 (2001).
21. Taeri, S., Brunner, D., Sigle, W., & Ruhle, M. Deformation Behavior of Strontium Titanate between Room Temperature and 1800K under Ambient Pressure. *Z. Metallkd.* **95** 433-446 (2004).
22. Takahashi, K., Ohtomo, A., Kawasaki, M., & Koinuma, H. Advanced Processing and Characterization of SrTiO3 Single Crystals and Bicrystals for High Tc Superconducting Film Substrate. *Mater. Sci. Eng. B.* **B41** 152-156 (1996).
23. Rhodes, W. H., & Kingery, W. D. Dislocation Dependence of Cationic Diffusion in SrTiO3. *J. Amer. Ceram. Soc.* **49** (10), 521-526 (1966).
24. Yamamoto, T., Hayashi, K., Ikuhara, Y., & Sakuma, T. Grain Boundary Structure and Electrical Properties in Nb-Doped SrTiO₃ Bicrystals. *Key Eng. Mater.* **181-182** 225-230 (2000).
25. Fitting, L., Thiel, S., Schmehl, A., Mannhart, J., & Muller, D. A. Subtleties in ADF imaging and spatially resolved EELS: A case study of low-angle twist boundaries in SrTiO3. *Ultramicroscopy.* **106** (11-12), 1053-1061 (2006).
26. Hughes, L. A., & van Benthem, K. Formation of SrTiO3 bicrystals using spark plasma sintering techniques. *Scr. Mater.* **118** 9-12 (2016).

